Nano Research
DOI 10.1007/s12274-015-0820-0
Research Article
ISSN 1998-0124
CN 11-5974/O4

Novel fabrication of copper nanowire/cuprous oxide-based semiconductor-liquid junction solar cells

Haitao Zhai, Ranran Wang (✉), Weiqi Wang, Xiao Wang, Yin Cheng, Liangjing Shi, Yangqiao Liu, and Jing Sun (✉)

The State Key Lab of High Performance Ceramics and Superfine Microstructure, Shanghai Institute of Ceramics, Chinese Academy of Sciences, 1295 Dingxi Road, Shanghai 200050, China

Received: 21 January 2015
Revised: 12 May 2015
Accepted: 20 May 2015

KEYWORDS
Cu nanowires, semiconductor-liquid junction solar cells, transparent electrodes, cuprous oxide

ABSTRACT

A Cu nanowire (NW)/cuprous oxide (Cu_2O)-based semiconductor-liquid junction solar cell with a greatly enhanced efficiency and reduced cost was assembled. The Cu NWs function as a transparent electrode as well as part of the Cu NWs/Cu_2O coaxial structures, which remarkably benefit the charge separation. The best solar cell reached a conversion efficiency as high as 1.92% under a simulated AM1.5G illumination, which is 106 times higher than that of cells based on fluorine-doped tin oxide and Cu_2O.

1 Introduction

The need for renewable energy has encouraged research on a variety of photovoltaic materials and structures, with a great emphasis on good performance and low cost. The stability of many inorganic semiconductors compared with other solar-cell technologies, such as organic solar cells [1], dye-sensitized solar cells [2], and perovskite solar cells [3–5], makes them attractive alternatives. However, low-cost, nontoxic, inorganic semiconductor solar-cell technologies have received comparatively less attention.

Cuprous oxide (Cu_2O) is a nontoxic and inexpensive semiconductor with a bandgap of 2 eV, which makes it suitable for solar-cell applications. A number of Cu_2O-based solar cells have been reported; however, their efficiencies are very low because of the charge recombination at the crystal boundary and the large resistance of Cu_2O [6–12]. For instance, Musselman et al. [7] deemed that the poor charge collection limits the performance of electrodeposited bilayer Cu_2O-ZnO solar cells and designed a nanowire (NW) architecture

Address correspondence to Jing Sun, jingsun@mail.sic.ac.cn; Ranran Wang, wangranran@mail.sic.ac.cn

to enhance the minority carrier collection, reporting an efficiency of 0.47%. Xie et al. [12] used an all-electrochemical approach to directly deposit ZnO NWs onto fluorine-doped tin oxide (FTO), followed by electrochemical doping with Ga to produce a heterojunction solar cell with Cu_2O, and reported an efficiency of 0.25%. Kazuya et al. [10] prepared Cu_2O with highly oriented {111} crystallites and achieved an efficiency of 1.43% using Cu_2O-ZnO. In recent years, semiconductor-liquid junction solar cells have attracted increasing attention [13–15]. They offer an opportunity to fabricate efficient solar cells based on Cu_2O. Lewis et al. [14] prepared liquid-junction solar cells with Cu_2O photoelectrodes and reported an efficiency of 1.5%. Shao et al. [15] prepared non-aqueous liquid-junction solar cells with Cu/Cu_2O photoelectrodes and achieved a remarkable efficiency of 3.13%. This large improvement in the efficiency was due to the Cu/Cu_2O structures, which not only greatly decrease the resistance of Cu_2O layer but also assist the charge separation.

However, previously reported Cu_2O-based solar cells mainly used FTO as transparent electrodes, which increased the total cost of the solar cells significantly. Metal-NW thin films, because of their high optical-electrical performance, superior flexibility, and low cost, have attracted considerable attention as alternatives [16–22]. Chung et al. [23] prepared $CuInSe_2$ solar cells with Ag NW-indium tin oxide (ITO) nanoparticle composite transparent electrodes and reported an efficiency of 10.3%. Song et al. [24] prepared organic solar cells with Ag NW transparent electrodes and reported an efficiency of 5.80%. Wiley et al. [21] prepared organic solar cells with Cu-Ni NW transparent electrodes and reported an efficiency of 4.9%.

Herein, we present a Cu NW/Cu_2O-based semiconductor-liquid junction solar cell. The Cu NWs act as a transparent electrode as well as part of the Cu NWs/Cu_2O coaxial structures, which remarkably benefit the charge separation. The best solar cell exhibited an open-circuit voltage (V_{OC}) of 0.69 V, a short-circuit current density (J_{SC}) of 5.03 mA/cm^2, a fill factor of 55.3%, and a conversion efficiency of 1.92% under a simulated AM1.5G illumination.

2 Experimental

2.1 Preparation of Cu NWs

To synthesize the Cu NWs, we used a solvothermal method that was previously reported by our research team [25, 26]. In a typical synthesis, 8.16 g of hexadecylamine (HDA) and 0.5 g of cetrimonium bromide (CTAB) were dissolved in a glass vial at 180 ℃. Next, 200 mg of copper acetylacetonate [$Cu(acac)_2$] was added and mixed evenly. Then, 5–7 μL of a Pt nanoparticle suspension was added as a catalyst. The Pt nanoparticles were synthesized as follows: 2 mg of platinous chloride was dispersed into 1.2 mL of ethylene glycol, added to 2.3 mL ethylene glycol, and maintained at 160 ℃ for 90 s. The mixtures were then maintained at 180 ℃ for 12 h, causing the formation of reddish cotton-like sheets that settled at the bottom. After rinsing with toluene several times, the NWs were placed in toluene.

2.2 Preparation of Cu NWs transparent electrode

The Cu NWs were dispersed in the toluene by bath sonication for 1–2 min and then filtered onto a nitrocellulose filter membrane. After the filtration, the filter membranes were transferred onto a glass slide film, dried in vacuum at 80 ℃ for 2 h, and then dipped in acetone for 30 min to dissolve the filter membrane, leaving Cu NW-based thin films on the glass slide. Finally, the films were treated with H_2 at 300 ℃ to remove the oxidized layers and the residual HDA on the surface [26].

2.3 Preparation of Cu NWs/Cu_2O photoanodes

Electrodepositions of Cu_2O were performed using a standard three-electrode cell where a Cu NW transparent electrode, a saturated calomel electrode, and platinum were used as the working, reference, and counter electrodes, respectively. The electrolyte was composed of cupric acetate (0.02 M) and acetic acid (0.08 M), to which a sodium hydroxide solution (0.8 M) was added to adjust the pH. The samples were deposited potentiostatically at –80 mV for 20 min, and the temperature was varied from 60 to 75 ℃. After each deposition, the obtained film was rinsed with

ethanol and then dried in a vacuum oven at 60 ˚C. For comparison, pure Cu_2O films were deposited on an FTO glass. Moreover, the effects of the pH and the deposition temperature were examined. The as-prepared samples were denoted as Cu NWs/Cu_2O-*x*-*y* or Cu_2O-*x*-*y*, where *x* = 5.2, 5.8, or 6.4 and *y* = 60, 65, or 70 represent the corresponding pH and deposition temperature (˚C), respectively.

2.4 Fabrication of the solar cells

The solar cells were composed of a photoanode, a platinum-sputtered FTO counter electrode, and a liquid electrolyte. The two electrodes were separated by a spacer. The internal space of the cells was filled with the electrolyte, which contained LiI (0.5 M), I_2 (0.05 M), and tert-butylpyridine (0.5 M) in acetonitrile.

2.5 Characterization of samples

The compositions of the photoanodes were investigated by X-ray diffraction (XRD, D/max2550V, Rigaku Tokyo, Japan) and energy dispersive spectrometry (EDS). The morphology was characterized by field-emission scanning electron microscopy (FE-SEM, Magellan 400, FEI, USA). The transmittance and absorption data were collected using a Lambda-950 UV–Vis spectrophotometer (PerkinElmer, Waltham, MA). The specular transmittance and the diffusive transmittance were measured with and without the integrating sphere. The current density-voltage (*J*–*V*) characteristics of the solar cells were measured using an electrochemical workstation (ModelCHI660C, CH) under an AM1.5G illumination (100 mW/cm^2, Model YSS-80A, Yamashita). The light source was a Xe lamp equipped with an AM1.5G filter. Prior to the measurements, an aperture mask was used to calibrate the cell area to 0.12 cm^2. The intensity of the incident light was calibrated to 100 mW/cm^2 with a standard Si solar cell. The electrochemical impedance spectroscopy (EIS) curves of the cells were measured in the frequency range of 0.1 Hz to 100 kHz under open-circuit conditions. The *J*–*V* curves were recorded by a Keithley Series 2400 System Source Meter Instrument in the stability test. A solar simulator (Newport) was used as the irradiation source to provide an AM1.5G illumination for the solar cells.

3 Results and discussion

Cu NWs with diameters of 60–80 nm and lengths over 50 μm were prepared by the method reported in our previous work [23, 24] and were constructed into thin films by a vacuum filtration method followed by an annealing treatment in H_2. Figure 1(a) shows the typical optical-electrical performance of the as-prepared Cu NW films, which exhibited sheet resistances of 27 and 10 Ω/sq at transmittances of 84% and 78%, respectively, at a wavelength of 550 nm. Although it is inferior to that of the best Ag NW electrodes and ITO conducting glass, this performance is far superior to that of electrodes based on carbon nanotubes (CNTs) and CNTs/graphene and comparable to that of all reported first-class Cu NW electrodes. The optical spectra of the Cu NW electrodes (with the transmittances of 90% and 70% at 550 nm) are shown in Fig. 1(b). The transmittance remained nearly constant over the whole visible range when the Cu NW film was thin, and an obvious decrease in the range of 400–580 nm occurred when the Cu NW film became thicker, owing to the enhanced absorption, reflection, and diffusion (scattered at an angle greater than the specularly transmitted light but less than 180°). The difference between the diffusive transmittance and the specular transmittance was approximately 3% and ~9% at a specular transmittance of 90% and 70%, respectively. Although the diffusive transmittance is undesirable for displays, it can increase the light capture in thin-film solar cells [27]. Figures 1(c) and 1(d) show SEM images of the Cu NW films with different transmittances, in which a continuous network formed by long, bendable Cu NWs is observed. The NWs fused together in the junction area after the annealing treatment, as observed in the inset of Fig. 1(c), which ensured the efficient charge transport between the NWs. As the thickness increased, the NW density increased, and the blank space among the NWs decreased. In this work, thick Cu NW films (generally with a transmittance of ~62%) were chosen as the transparent electrodes to ensure the dense deposition of the Cu_2O, as they can only be deposited in the conductive area during the electrodeposition process. The inset in Fig. 1(d) shows a photograph of the Cu NW electrode used in this work.

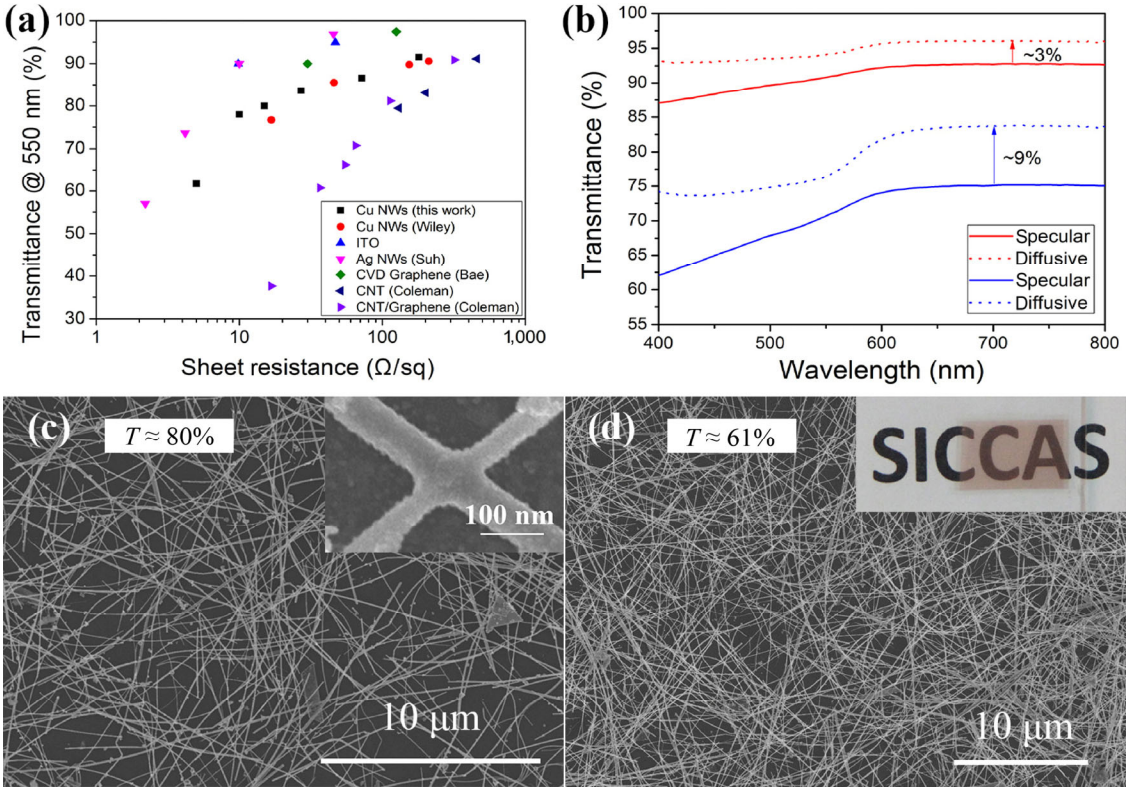

Figure 1 (a) Plot of the transmittance (at a wavelength of 550 nm) with respect to the sheet resistance for films of Cu NWs, Ag NWs, ITO, graphene, and CNTs. The optical spectrum (b) and SEM images (c) and (d) of the Cu NW electrode. The red and blue curves of (b) are two different Cu NW electrodes with transmittances of 90% and 70% at 550 nm. The inside images of (c) and (d) show the magnified junction and a digital photograph of the Cu NWs transparent electrode.

The Cu_2O layer was directly electrodeposited onto the freshly made Cu NW electrodes. This mainly comprised two steps: the cathodic reduction of Cu^{2+} ions to Cu^{+} ions and the precipitation of Cu_2O due to the solubility limitation of the Cu^{+} ions [28, 29]. The experimental conditions involving the pH and electrodeposition temperature have a great influence on the composition of the samples. Figure 2 shows the XRD pattern of the as-deposited photoanode samples for different pH and temperature values. All the peaks can be ascribed to Cu and Cu_2O [15, 28, 30], and no peak of CuO was observed. The sharp peaks indicate that the Cu_2O was well crystalized in all the samples. The Raman spectra (Fig. S2 in the Electronic Supplementary Material (ESM)) also demonstrate the formation of Cu_2O in addition to the CuO [31]. For comparison, electrodeposition was also conducted on an FTO glass at 60 ˚C and a pH of 5.8. Peaks attributed to Cu_2O and FTO were observed in its XRD pattern, without the appearance of Cu. This proves that under

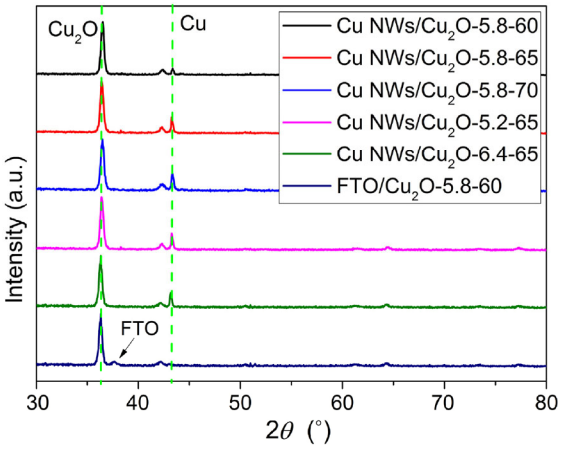

Figure 2 XRD patterns of the different photoanodes.

the condition of 5.8-60 (a pH of 5.8 and a temperature of 60 ˚C), no Cu (0) is electrodeposited. Therefore, the Cu peak in the XRD pattern of the Cu NW/Cu_2O-5.8-60 should exclusively originate from the Cu NW electrode. Notably, the intensity of the Cu peaks increased as the deposition temperature increased

and as the pH decreased. This indicates that the contents of Cu (0) are increased by increasing the deposition temperature or reducing the pH.

The top view and cross-section SEM images of the anode are shown in Figs. 3(a)–3(f). When the pH is 5.8, large prismatic Cu_2O crystals grow along the Cu NWs and tightly wrap them, eventually forming a Cu NW/cuprous oxide coaxial structure. The cross-section image and the element line-scan analysis clearly indicate the Cu_2O-wrapped Cu NW structure, and the Cu_2O-Cu layer thickness is ~900 nm. When the temperature was increased, small polyhedral Cu_2O crystals formed in the blank space among the Cu NWs-Cu_2O coaxial structures (Figs. 3(b) and 3(c)).

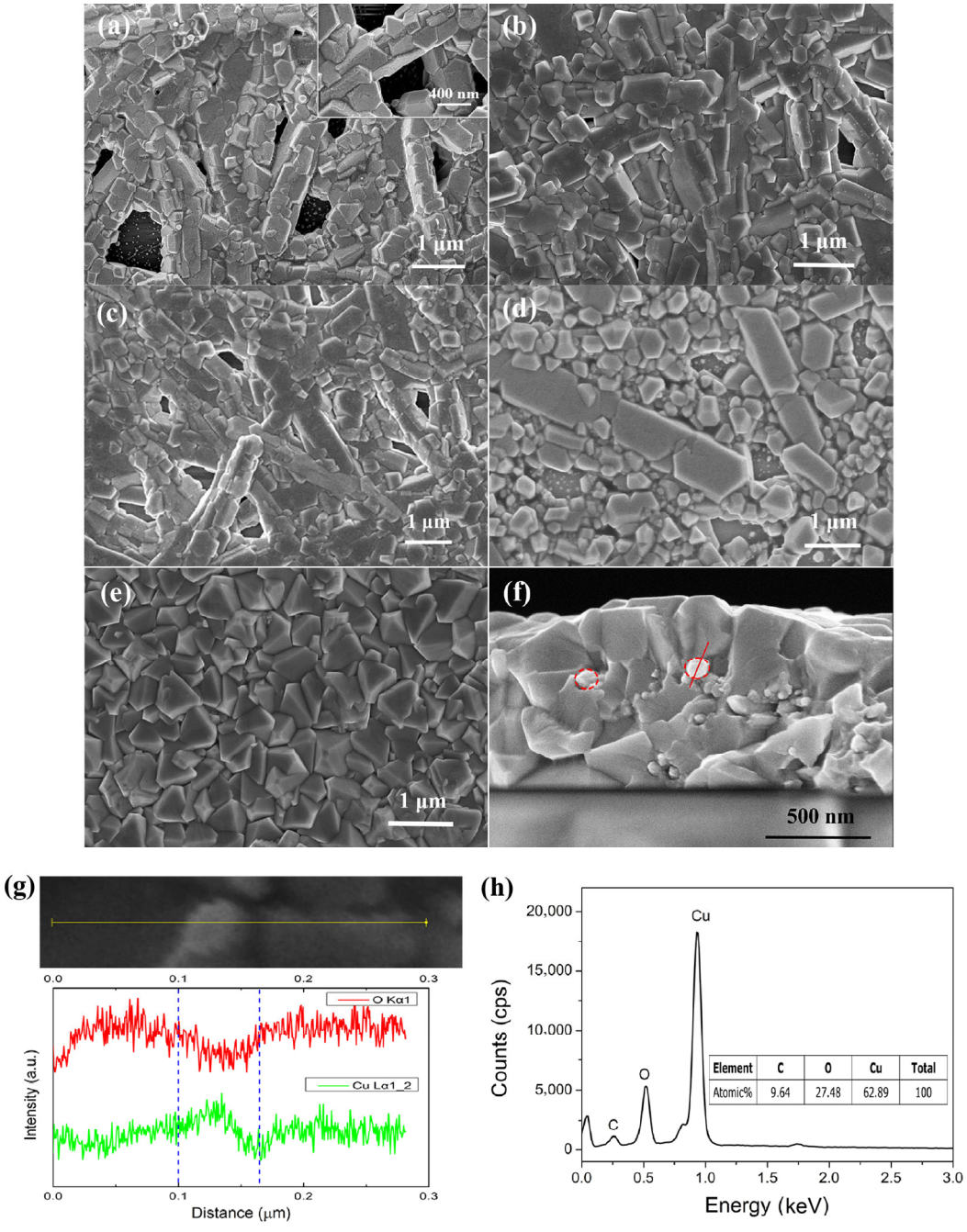

Figure 3 Top-view SEM images of the photoanodes Cu NWs/Cu_2O-5.8-60 (a), Cu NWs/Cu_2O-5.8-65 (b), Cu NWs/Cu_2O-5.8-70 (c), Cu NWs/Cu_2O-5.2-65 (d), and FTO/Cu_2O-5.8-60 (e), cross-section SEM image of the photoanode Cu NWs/Cu_2O-5.8-65 (f), EDS line scan of a Cu NW and the surrounding Cu_2O (g), EDS of the Cu_2O (h).

The same phenomenon was also observed when the electrodeposition pH was reduced. When the pH was reduced to 5.2, only a few large prismatic Cu_2O crystals were observed along the Cu NWs; most of the Cu_2O crystals were smaller, having the morphology of a polyhedron, and uniformly deposited on the Cu NW film (Fig. 3(d)). The difference in microstructure of the Cu_2O layer is primarily attributed to the precipitation of the Cu (0) during the electrodeposition. As is well-known, materials can only be deposited in the conductive area during the electrodeposition process. Regarding the Cu NW electrodes, the charges are specifically transported along the Cu NWs, leaving a blank space among the NW insulation. This explains why the Cu_2O mainly grew along the Cu NWs in the sample of Cu NWs/Cu_2O-5.8-60. As the deposition temperature increased and the pH decreased, the Cu (0) precipitated, which broadened the conductive area, yielding increasing depositions of Cu_2O in the blank space. Comparably, a homogeneous layer of Cu_2O crystals with the morphology of a random polyhedron was deposited when FTO was used as the electrode (Fig. 3(e)), as the full surface of the FTO was homogeneously and continuously conductive. Figure 3(g) shows an EDS line scan of a Cu NWs and the surrounding Cu_2O. Here, the count of O decreases and the count of Cu increases through the Cu NW. EDS reveals that the Cu_2O has an atomic ratio of Cu to O of 2:1 (Fig. 3(h)).

Figure 4 shows the absorption spectra of the as-prepared photoanodes. All of them have a strong absorption in the wavelength range of 400 to 500 nm because the bandgap of the Cu_2O is ~2.0 eV. Clearly, the Cu NWs/Cu_2O photoanodes have a better light-harvesting ability than FTO/Cu_2O ones. It is presumed that the Cu NWs/Cu_2O coaxial structure contributes to the light harvesting because of the longer optical path arising from the scattering of the incident light by the Cu NWs. In addition to the Cu NWs, the electrodeposited Cu metals also facilitated the optical absorption of the photoanodes. Compared with the Cu NWs/Cu_2O-5.8-60, in which there was no electrodeposited Cu metal, the photoanodes deposited under a lower pH and higher temperature exhibited an enhanced optical absorption. The photoanodes deposited under the conditions of 5.8-65 and 5.2-65

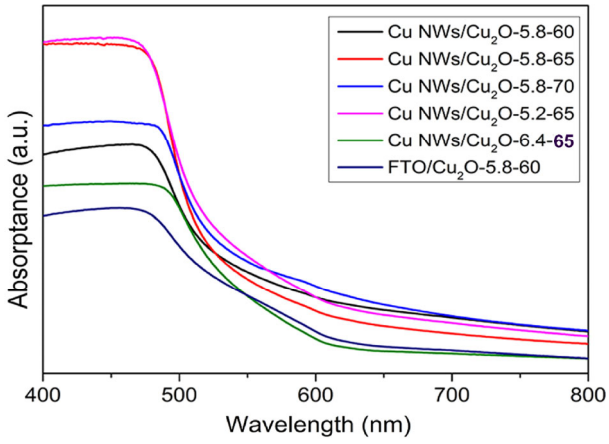

Figure 4 Absorption spectra of the as-prepared photoanodes.

exhibited the highest absorption, and the absorption decreased noticeably when the deposition temperature was increased to 70 °C. This is reasonable, as the deposition electrical quantity is constant, and the increased deposition of Cu metal will result in the decreased deposition of Cu_2O.

Sandwich-type solar cells were fabricated with the as-prepared photoanodes, and their performances were evaluated by collecting the *J*–*V* curves under an AM1.5G illumination. The characteristics are presented in Fig. 5, and the parameters for the cells prepared from the four different photoanodes are reported in Table 1. When FTO/Cu_2O-5.8-60 was used as the photoanode, the *J*–*V* curves of the cells had a diagonal appearance. The J_{SC} and V_{OC} were both very low: 0.12 mA/cm² and 0.36 V, respectively. The efficiency (η) was only 0.0115%, which is similar to the value of 0.013% reported by Shao et al. [15]. The series

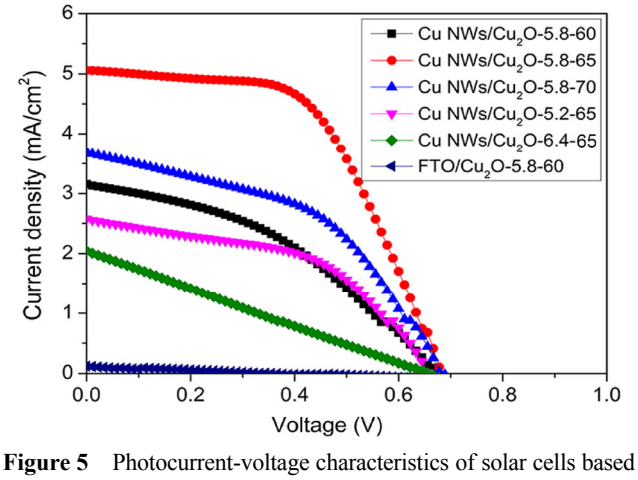

Figure 5 Photocurrent-voltage characteristics of solar cells based on different photoanodes under the AM1.5G illumination.

Table 1 Characteristics of the solar cells based on the different photoanodes

Photoanodes	J_{SC} (mA/cm^2)	V_{OC} (V)	FF (%)	η (%)	R_S (Ω)	R_{SH} (Ω)
Cu NWs/Cu_2O-5.8-60	3.26	0.71	35.98	0.836	1,590	5,050
Cu NWs/Cu_2O-5.8-65	5.03	0.69	55.31	1.922	486	19,080
Cu NWs/Cu_2O-5.8-70	3.67	0.7	45.79	1.172	822	4,664
Cu NWs/Cu_2O-5.2-65	2.57	0.67	48.43	0.833	867	5,556
Cu NWs/Cu_2O-6.4-65	2.04	0.66	24.35	0.327	2,785	2,772
FTO/Cu_2O-5.8-60	0.12	0.36	26.62	0.0115	22,137	13,481

resistance (R_S) was 22,137 Ω, and the shunt resistance (R_{SH}) was 13,481 Ω. The giant resistance of the pure Cu_2O film is primarily responsible for the bad performance, as it results in a high R_S of the corresponding cells and thus causes a great loss of photovoltaic efficiency. When Cu NW films are used as the electrodes, the overall performance increases sharply. A power conversion efficiency as high as 1.92% was obtained using Cu NWs/Cu_2O-5.8-65 as the photoanode, which is higher than that of most reported Cu_2O liquid-junction solar cells [14, 32] and ZnO/Cu_2O solar cells [7, 10]. The J_{SC} and V_{OC} both increased significantly, to 5.03 mA/cm^2 and 0.69 V, respectively. The V_{OC} value of ~0.7 V is far higher than the reported V_{OC} values of 0.415–0.535 V for Cu_2O/ZnO [10], 0.4 V for Cu_2O/Al-doped ZnO [33], and 0.27 V for Cu_2O/ITO [34]. The higher V_{OC} is mainly attributed to the superior interface contact and energy-level matching in the Cu NWs/Cu_2O coaxial structures.

To further understand the inner operation process of the solar cells, EIS was performed under a light illumination. The inset image shown in Fig. 6(a) discloses that in the case of the cells based on FTO/Cu_2O-5.8-60, the Nyquist plot only consists of a low-frequency arc. In contrast, the Nyquist plots of the cells based on Cu NWs/Cu_2O all comprise one arc and one line, as shown in Fig. 6(a). The arcs are compressed because of the inhomogeneity of the electrical properties of the measured interface [15, 35]. The shape and size of the compressed semicircle are related to the photo-injected electron transport in the Cu NWs/Cu_2O film or the back reaction at the Cu NWs/Cu_2O-electrolyte interface, and the smaller semicircle represents the lower charge-transport resistance. Compared with the FTO/Cu_2O-5.8-60, the semicircles of Cu NWs/Cu_2O are reduced, indicating the great decrease in the charge-transport resistance caused by introducing the Cu NWs. This is on one hand attributed to the outstanding conducting performance of the Cu NW network, whose sheet resistance of 5 Ω/sq is lower than that of FTO glass. On the other hand, the distinctive Cu NWs-Cu_2O coaxial structure considerably facilitated

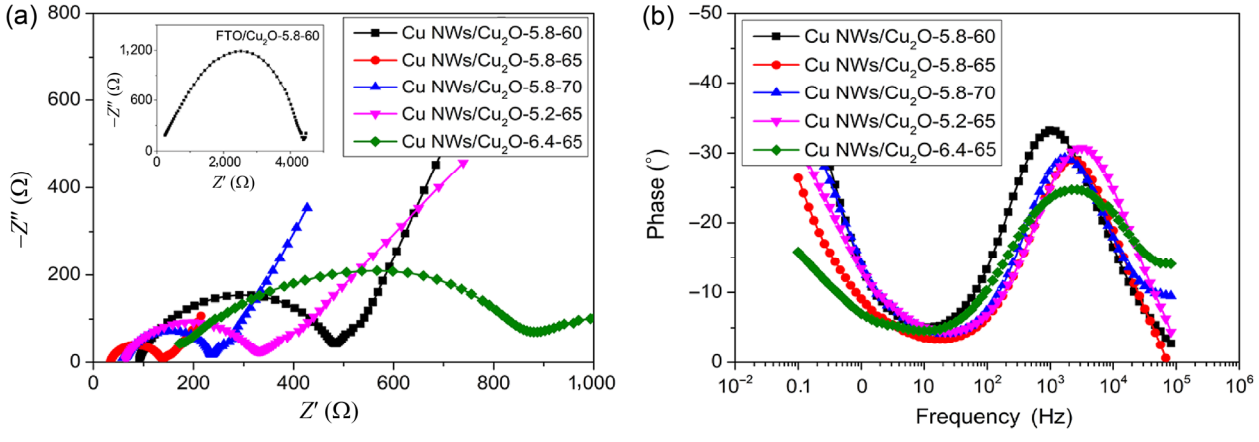

Figure 6 Electrochemical impedance spectra of cells with different electrodes. (a) Nyquist plots, (b) Bode plots. The inside images are the corresponding characteristics of FTO/Cu_2O-5.8-60.

the charge separation and transport. Among the cells based on the Cu NWs/Cu_2O photoanodes, the Cu NWs/Cu_2O-5.8-65 cell had the smallest semicircle, indicating the best charge transfer ability. The Cu NWs/Cu_2O-5.8-70 cell had the second-best charge-transport performance, followed closely by the Cu NWs/Cu_2O-5.2-65 cell. These three cells exhibited a lower charge-transfer resistance than the Cu NWs/Cu_2O-5.8-60 and Cu NWs/Cu_2O-6.4-65 cells owing to the electrodeposition of the Cu metal. The order of the charge-transport ability is completely consistent with the order of the power conversion efficiency of the cells, confirming the aforementioned decisive impact of the conductance of the photoanodes.

In addition to charge transport, the Nyquist plot also embodies the diffusion of ions. The line in the low-frequency range is related to the Warburg diffusion of the ions in the electrolyte, and the higher slope of the line represents the faster diffusion of the ions, according to previous reports [36]. As shown in Fig. 6(a), the cells deposited at a pH of 5.8 have an apparently higher slope than the cells deposited at 5.2 and 6.4, indicating the superiority of the Cu NWs-Cu_2O coaxial structure for facilitating the diffusion of ions.

Figure 6(b) shows the Bode plots of the cells with different photoanodes. Here, the high-frequency peak of the Cu/Cu_2O-5.8-60 cell is shifted to a lower frequency compared with the other cells, suggesting that solar cells based on Cu/Cu_2O-5.8-60 have the smallest charge recombination [37]. This shows that although the electrodeposition of the Cu metal can reduce the global resistance of the cells, too much Cu and too many small Cu_2O crystals increases the charge recombination, which explains the relatively inferior performance of the Cu NWs/Cu_2O-5.2-65 cells.

According to the experimental results and relevant reports [15, 38, 39], the possible charge-transfer mechanism in the Cu NWs/Cu_2O interface and the operation principle of the cells are proposed as shown in Fig. 7. The Fermi level of the Cu_2O is located at a more negative level than that of the Cu metal. When Cu_2O is in contact with Cu, the band structure of the Cu_2O (both the valence band (VB) and the conduction band (CB)) is bent, as shown in Fig. 7. When Cu_2O crystals contact the electrolyte solution, the electrons are transported from the Cu_2O to the vacant level of

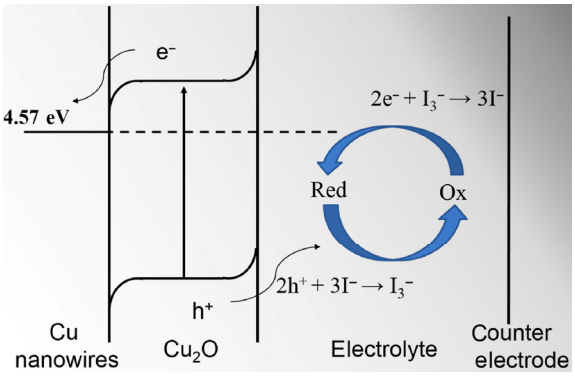

Figure 7 Schematic illustration of the possible charge-transfer mechanism in the Cu NWs/Cu_2O interface and the operation principle of the cells.

the electrolyte solution, making the Cu_2O positively charged and the nearby electrolyte solution negatively charged. As a result, the band structure of the Cu_2O is bent, as shown in Fig. 7. This curved portion of the band structure is called a space-charge layer or depletion layer. Under this condition, upon irradiation by photons whose energy is larger than the bandgap of the semiconductor ($h\nu > Eg$), the excitation of the electrons from the VB to CB in the Cu_2O occurs, leaving holes in the VB. The electron and the hole form an exciton, which is usually short-lived and recombines if there is no driving force to separate them. However, when the band structure is bent as shown in Fig. 7, the hole can migrate toward the Cu_2O/electrolyte interface, and the electron can migrate toward the Cu NWs/Cu_2O interface; thus the hole and the electron are effectively separated. Furthermore, the Cu NWs act as a direct conductive pathway, allowing fast charge transportation, which tremendously suppresses the charge recombination and correspondingly enhances the efficiency of the cells. When the holes migrate to the Cu_2O/electrolyte interface, they oxidize the donor (I^-) to I_3^-, which diffuses to the counter and is reduced by the catalyst, completing the cycle.

The stability test was conducted with a short circuit for 30 min under full-sun conditions. As shown in Fig. 8(a), after an AM1.5G illumination for 30 min, the efficiency of the Cu NWs/Cu_2O-5.8-60 solar cell exhibited a slight increase due to the augmentation of the fill factor from 36.0% to 39.3%. The V_{OC} and J_{SC} remained almost the same. We propose that the increase in the efficiency was caused by the activation

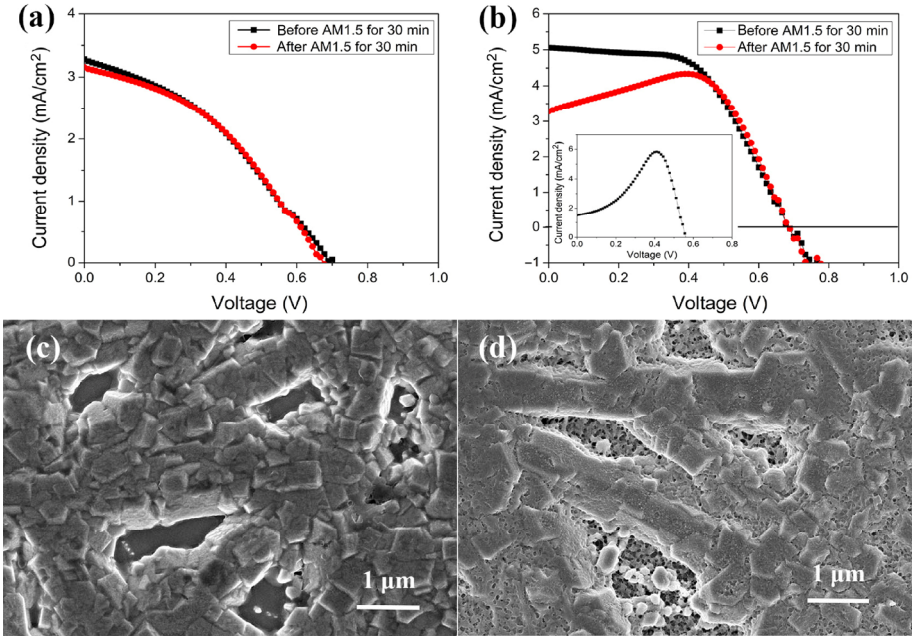

Figure 8 Photocurrent-voltage characteristics of the photoanodes Cu NWs/Cu_2O-5.8-60 (a) and Cu NWs/Cu_2O-5.8-65 (b) before and after illumination for 30 min; SEM images of the photoanodes Cu NWs/Cu_2O-5.8-60 (c) and Cu NWs/Cu_2O-5.8-65 (d) after illumination for 30 min. The inset image of (b) shows the *J*–*V* curves of the Cu sheet reacting with the electrolyte without illumination.

of the photoanode during the illumination. Unlike the case of Cu NWs/Cu_2O-5.8-60, a peak appeared near 0.4 V after 30 min of exposure to the full-sun conditions with a short circuit for the Cu NWs/Cu_2O-5.8-65 cells. The inset image of Fig. 8(b) represents the *J*–*V* curves of the Cu sheet reacting with the electrolyte without illumination, which is similar to the case of the Cu NWs/Cu_2O-5.8-65 cell after illumination. The peak near 0.4 V is attributed to the corrosion of the Cu, which occurs during the electrodeposition. To confirm this conjecture, SEM images of the Cu NWs/Cu_2O-5.8-60 and Cu NWs/Cu_2O-5.8-65 cells after illumination for 30 min were obtained, as shown in Figs. 8(c) and 8(d).

Corrosion clearly occurred in Cu NWs/Cu_2O-5.8-65 (Fig. 8(d)), while the compact Cu_2O-Cu NW structures remained as Cu NWs/Cu_2O-5.8-60 (Fig. 8(c)). This is because the Cu NW network was closely wrapped by the Cu_2O layers and hardly directly contacted the electrolyte, thus protecting the NWs from corrosion. Nevertheless, some of the deposited Cu metal was exposed in the electrolyte and corroded by I_3^-.

Compared with TiO_2-based dye-sensitized solar cells (DSSCs), the efficiency of our Cu NWs/Cu_2O based semiconductor-liquid junction solar cells is low, which is attributed to three main reasons. First, traditional DSSCs use commercial FTO, which has a far higher transmittance—usually over 85%—as a transparent electrode. Second, only light with wavelength less than 480 nm can be absorbed by Cu_2O, whereas the spectrum absorbed by DSSCs is almost the entire visible region. Third, large numbers of defects in the grain boundary may cause the charge recombination of the photogenerated charges. In a future work, the diameter, length, and pattern of the Cu NWs will be optimized to obtain a higher transmittance and lower sheet resistance in order to improve the efficiency of the solar cells. In addition, varying the crystallite orientation of the Cu_2O may be another effective approach to enhance the photoelectric performance [10, 34].

4 Conclusions

We fabricated Cu NWs-Cu_2O semiconductor-liquid junction solar cells with a greatly enhanced efficiency and reduced cost. The Cu NWs-Cu_2O coaxial structure contributes to light harvesting and facilitates charge separation and transportation, which are the key factors for improving the efficiency of solar cells. An

efficiency up to 1.92% was obtained using Cu NWs-Cu_2O-5.8-65 photoanodes, which is 106 times higher than that obtained using cells based on FTO-Cu_2O-5.8-65. Furthermore, a band-bent mechanism was proposed to illustrate the charge transfer in the Cu NWs-Cu_2O-electrolyte interface. We proposed a method to enhance the efficiency of the Cu_2O-based solar cells and reduce their cost. Our findings may shed light on new ways to fabricate cost-effective solar cells.

Acknowledgements

This work was financially supported by the National Basic Research Program of China (No. 2012CB932303), the National Natural Science Foundation of China (No. 61301036), Shanghai Municipal Natural Science Foundation (Nos. 13ZR1463600 and 13XD1403900) and the Innovation Project of Shanghai Institute of Ceramics.

Electronic Supplementary Material: Supplementary material (schematic illustration of the sites to be measured and the transmittance vs. sheet resistance for Cu NWs films, and Raman spectra of the different photoanodes) is available in the online version of this article at http://dx.doi.org/ 10.1007/s12274-015-0820-0.

References

[1] Li, G.; Zhu, R.; Yang, Y. Polymer solar cells. *Nat. Photonics* **2012**, *6*, 153–161.

[2] Costa, R. D.; Lodermeyer, F.; Casillas, R.; Guldi, D. M. Recent advances in multifunctional nanocarbons used in dye-sensitized solar cells. *Energy Environ. Sci.* **2014**, *7*, 1281–1296.

[3] Docampo, P.; Ball, J. M.; Darwich, M.; Eperon, G. E.; Snaith, H. J. Efficient organometal trihalide perovskite planar-heterojunction solar cells on flexible polymer substrates. *Nat. Commun.* **2013**, *4*, 2761.

[4] Xing, G. C.; Mathews, N.; Sun, S. Y.; Lim, S. S.; Lam, Y. M.; Gratzel, M.; Mhaisalkar, S.; Sum, T. C. Long-range balanced electron- and hole-transport lengths in organic-inorganic $CH_3NH_3PbI_3$. *Science* **2013**, *342*, 344–347.

[5] Hodes, G.; Cahen, D. Perovskite cells roll forward. *Nat. Photonics* **2014**, *8*, 87–88.

[6] Yuhas, B. D.; Yang, P. D. Nanowire-based all-oxide solar cells. *J. Am. Chem. Soc.* **2009**, *131*, 3756–3761.

[7] Musselman, K. P.; Wisnet, A.; Iza, D. C.; Hesse, H. C.; Scheu, C.; MacManus-Driscoll, J. L.; Schmidt-Mende, L. Strong efficiency improvements in ultra-low-cost inorganic nanowire solar cells. *Adv. Mater.* **2010**, *22*, E254–E258.

[8] Cui, J. B.; Gibson, U. J. A simple two-step electrodeposition of Cu_2O/ZnO nanopillar solar cells. *J. Phys. Chem. C.* **2010**, *114*, 6408–6412.

[9] Cheng, K.; Li, Q. Q.; Meng, J.; Han, X.; Wu, Y. Q.; Wang, S. J.; Qian, L.; Du, Z. L. Interface engineering for efficient charge collection in Cu_2O/ZnO heterojunction solar cells with ordered ZnO cavity-like nanopatterns. *Sol. Energy Mater. Sol. Cells* **2013**, *116*, 120–125.

[10] Fujimoto, K.; Oku, T.; Akiyama, T. Fabrication and characterization of ZnO/Cu_2O solar cells prepared by electrodeposition. *Appl. Phys. Express* **2013**, *6*, 086503.

[11] Hsu, Y.-K.; Lin, H.-H.; Wu, J.-R.; Chen, M.-H.; Chen, Y.-C.; Lin, Y.-G. Electrochemical growth and characterization of a p-Cu_2O thin film on n-ZnO nanorods for solar cell application. *RSC Adv.* **2014**, *4*, 7655–7659.

[12] Xie, J. L.; Guo, C. X.; Li, C. M. Ga doping to significantly improve the performance of all-electrochemically fabricated Cu_2O-ZnO nanowire solar cells. *Phys. Chem. Chem. Phys.* **2013**, *15*, 15905–15911.

[13] Jose, R.; Thavasi, V.; Ramakrishna, S. Metal oxides for dye-sensitized solar cells. *J. Am. Ceram. Soc.* **2009**, *92*, 289–301.

[14] Xiang, C. X.; Kimball, G. M.; Grimm, R. L.; Brunschwig, B. S.; Atwater, H. A.; Lewis, N. S. 820 mV open-circuit voltages from Cu_2O/CH_3CN junctions. *Energy Environ. Sci.* **2011**, *4*, 1311–1318.

[15] Shao, F.; Sun, J.; Gao, L.; Luo, J. Q.; Liu, Y. Q.; Yang, S. W. High efficiency semiconductor-liquid junction solar cells based on Cu/Cu_2O. *Adv. Funct. Mater.* **2012**, *22*, 3907–3913.

[16] Rathmell, A. R.; Bergin, S. M.; Hua, Y. L.; Li, Z.-Y.; Wiley, B. J. The growth mechanism of copper nanowires and their properties in flexible, transparent conducting films. *Adv. Mater.* **2010**, *22*, 3558–3563.

[17] Hu, L. B.; Kim, H. S.; Lee, J. Y.; Peumans, P.; Cui, Y. Scalable coating and properties of transparent, flexible, silver nanowire electrodes. *ACS Nano* **2010**, *4*, 2955–2963.

[18] Li, L.; Yu, Z. B.; Hu, W. L.; Chang, C.-H.; Chen, Q.; Pei, Q. B. Efficient flexible phosphorescent polymer light-emitting diodes based on silver nanowire-polymer composite electrode. *Adv. Mater.* **2011**, *23*, 5563–5567.

[19] Lim, D. C.; Kim, K.-D.; Park, S.-Y.; Hong, E. M.; Seo, H. O.; Lim, J. H.; Lee, K. H.; Jeong, Y.; Song, C.; Lee, E. et al. Towards fabrication of high-performing organic photovoltaics: New donor-polymer, atomic layer deposited thin buffer layer and plasmonic effects. *Energy Environ. Sci.* **2012**, *5*, 9803–9807.

[20] Guo, H. Z.; Lin, N.; Chen, Y. Z.; Wang, Z. W.; Xie, Q. S.; Zheng, T. C.; Gao, N.; Li, S. P.; Kang, J. Y.; Cai, D. J. et al. Copper nanowires as fully transparent conductive electrodes. *Sci. Rep.* **2013**, *3*, 2323.

[21] Stewart, I. E.; Rathmell, A. R.; Yan, L.; Ye, S. R.; Flowers, P. F.; You, W.; Wiley, B. J. Solution-processed copper-nickel nanowire anodes for organic solar cells. *Nanoscale* **2014**, *6*, 5980–5988.

[22] Rathmell, A. R.; Nguyen, M.; Chi, M. F.; Wiley, B. J. Synthesis of oxidation-resistant cupronickel nanowires for transparent conducting nanowire networks. *Nano Lett.* **2012**, *12*, 3193–3199.

[23] Chung, C.-H.; Song, T.-B.; Bob, B.; Zhu, R.; Duan, H.-S.; Yang, Y. Silver nanowire composite window layers for fully solution-deposited thin-film photovoltaic devices. *Adv. Mater.* **2012**, *24*, 5499–5504.

[24] Song, M.; You, D. S.; Lim, K.; Park, S.; Jung, S.; Kim, C. S.; Kim, D.-H.; Kim, D.-G.; Kim, J.-K.; Park, J. et al. Highly efficient and bendable organic solar cells with solution-processed silver nanowire electrodes. *Adv. Funct. Mater.* **2013**, *23*, 4177–4184.

[25] Cheng, Y.; Wang, S. L.; Wang, R. R.; Sun, J.; Gao, L. A. Copper nanowire based transparent conductive films with high stability and superior stretchability. *J. Mater. Chem. C.* **2014**, *2*, 5309–5316.

[26] Zhang, D. Q.; Wang, R. R.; Wen, M. C.; Weng, D.; Cui, X.; Sun, J.; Li, H. X.; Lu, Y. F. Synthesis of ultralong copper nanowires for high-performance transparent electrodes. *J. Am. Chem. Soc.* **2012**, *134*, 14283–14286.

[27] Hu, L. B.; Zheng, G. Y.; Yao, J.; Liu, N. A.; Weil, B.; Eskilsson, M.; Karabulut, E.; Ruan, Z. C.; Fan, S. H.; Bloking, J. T. et al. Transparent and conductive paper from nanocellulose fibers. *Energy Environ. Sci.* **2013**, *6*, 513–518.

[28] McShane, C. M.; Choi, K.-S. Photocurrent enhancement of n-type Cu_2O electrodes achieved by controlling dendritic branching growth. *J. Am. Chem. Soc.* **2009**, *131*, 2561–2569.

[29] Wang, L. C.; Tao, M. Fabrication and characterization of p-n homojunctions in cuprous oxide by electrochemical deposition. *Electrochem. Solid-State Lett.* **2007**, *10*, H248–H250.

[30] Tang, Y. W.; Chen, Z. G.; Jia, Z. J.; Zhang, L. S.; Li, J. L. Electrodeposition and characterization of nanocrystalline cuprous oxide thin films on TiO_2 films. *Mater. Lett.* **2005**, *59*, 434–438.

[31] Zhang, Y. Z.; Zhao, Y. Q.; Li, F. Y.; Sun, Z. X.; Xu, L.; Guo, X. L. Photovoltaic performance enhancement of Cu_2O photocathodes by electrostatic adsorption of polyoxometalate on Cu_2O crystal faces. *RSC Adv.* **2014**, *4*, 1362–1365.

[32] Mahalingam, T.; Chitra, J. S. P.; Chu, J. P.; Moon, H.; Kwon, H. J.; Kim, Y. D. Photoelectrochemical solar cell studies on electroplated cuprous oxide thin films. *J. Mater. Sci. - Mater. Electron.* **2006**, *17*, 519–523.

[33] Tadatsugu, M.; Hideki, T.; Takahiro, S.; Toshihiro, M.; Hirotoshi, S. High-efficiency oxide heterojunction solar cells using Cu_2O sheets. *Jpn. J. Appl. Phys.* **2004**, *43*, L917.

[34] Sears, W. M.; Fortin, E.; Webb, J. B. Indium tin oxide/Cu_2O photovoltaic cells. *Thin Solid Films* **1983**, *103*, 303–309.

[35] Musselman, K. P.; Marin, A.; Wisnet, A.; Scheu, C.; MacManus-Driscoll, J. L.; Schmidt-Mende, L. A novel buffering technique for aqueous processing of zinc oxide nanostructures and interfaces, and corresponding improvement of electrodeposited ZnO-Cu_2O photovoltaics. *Adv. Funct. Mater.* **2011**, *21*, 573–582.

[36] Li, B. H.; Han, C. P.; He, Y.-B.; Yang, C.; Du, H. D.; Yang, Q.-H.; Kang, F. Y. Facile synthesis of $Li_4Ti_5O_{12}$/C composite with super rate performance. *Energy Environ. Sci.* **2012**, *5*, 9595–9602.

[37] Heng, L. P.; Wang, X. Y.; Yang, N. L.; Zhai, J.; Wan, M. X.; Jiang, L. p-n-junction-based flexible dye-sensitized solar cells. *Adv. Funct. Mater.* **2010**, *20*, 266–271.

[38] Assimos, J. A.; Trivich, D. Photovoltaic properties and barrier heights of single-crystal and polycrystalline Cu_2O-Cu contacts. *J. Appl. Phys.* **1973**, *44*, 1687–1693.

[39] Kaneko, M.; Ueno, H.; Nemoto, J. Schottky junction/ohmic contact behavior of a nanoporous TiO_2 thin film photoanode in contact with redox electrolyte solutions. *Beilstein J. Nanotechnol.* **2011**, *2*, 127–134.